



Modeling and simulation of friction stir welding process: A neural approach

Devendra Kumar Chaturvedi *, Atul Suri

Faculty of Engineering, Dayalbagh Educational Institute (Deemed to be Univ.), India

* Corresponding Author: dkchaturvedi@dei.ac.in

ARTICLE INFO

ABSTRACT

Article history

Received: September 9, 2023

Revised: November 18, 2023

Accepted: February 17, 2024

Keywords

Vertical axis Friction Stir;
Safe bending strength;
Bending toughness;
Flexible neural network model;
Optimization.

Friction Stir Welding (FSW) stands out as a groundbreaking method in solid-state joining for aluminum alloys, presenting an innovative way to achieve joints of exceptional quality. This research delves into the application of FSW for bonding, focusing on plates that are 6mm thick and made from aluminum alloys Al6063, Al5083, and AL6061, aiming to produce a variety of FSW joints. To evaluate the quality of these joints, the study compares mechanical properties such as tensile strength, safe bending strength, and bending toughness necessary for achieving a 90° bend. The investigation leverages welding data to formulate a neural model, starting with using a conventional feedforward neural model (CFNM). It tackles the limitations of CFNM, including its intensive training requirements and the challenge of dealing with unknown configurations, by proposing a new, more adaptable neural network model known as FNNM. When comparing the two models, it becomes evident that CFNM is constrained by a root mean square error (RMSE) of 7-15%, whereas FNNM marks a significant improvement with a minimal RMSE of 1-3%. This indicates that FNNM improves accuracy and effectively navigates the complexities of modeling with unknown parameters. Through this study, insightful contributions are made to understanding FSW in joining aluminum alloys and developing an advanced neural model capable of predicting the outcomes of welding with greater precision.

This is an open-access article under the [CC-BY-SA](https://creativecommons.org/licenses/by-sa/4.0/) license.



1. Introduction

In 1991, the United Kingdom's Welding Institute (TWI) introduced friction stir welding (FSW) as a solid-state joining method [1-7]. Aluminum and copper, chosen for their suitable mechanical, thermal, and electrical properties, are environmentally friendly and recyclable, making them ideal for structural applications [8-10]. Combining copper with lightweight materials like aluminum is essential to create lightweight, cost-effective components without compromising essential properties [11]. However, welding dissimilar materials can result in defects and intermetallic compounds (IMCs), affecting weld quality [12]. Solid-state joining processes such as explosive welding, friction welding, and roll welding have been used to address this, but FSW stands out by eliminating defects like porosities, alloy segregations, and grain boundary cracks [13-15].

FSW utilizes a non-consumable, revolving tool with a specially designed pin/probe and shoulder. Joint failures in FSW of Al-Cu are often attributed to hard and brittle IMCs in the thermo-mechanically affected zone (TMAZ), with joints failing through the nugget or TMAZ [16,17].

Various FSW parameters, such as tool geometry, design, tilt angle, base plate position, rotational speed, welding speed, and plunge force, influence joint quality [18,19]. However, limited research exists on the impact of FSW tool geometry and design for joining Al to Cu. Similarly, while there is literature on the effect of different pin profiles on material movement and joint quality during the FSW of some materials, there is a lack of similar studies for dissimilar nonferrous materials [20,21].

The quality of FSW joints depends upon many parameters besides the material and its properties, such as tool-related parameters, i.e., tool speed (rpm), the shape of the tool, the relative motion of the job piece, and tool (i.e., feed rate). Hence, it is necessary to optimize these parameters. Reynolds et al. [22] studied these parameters' effect on FSW quality. Previous studies [23-40] have explored the issue of parameter optimization by employing a variety of methodologies, including Analysis of Variance (ANOVA), thermo-mechanical finite element modeling, Grey Relational Analysis, Taguchi optimization, Genetic Algorithms (GA), Modified Differential Evolution, Artificial Neural Networks (ANN), Adaptive Neuro-Fuzzy Inference System (ANFIS), and their respective integrations, among others. These approaches have been applied to both similar and dissimilar materials. Aluminum plates are crucial in shipbuilding and naval applications, where bending loads precede tensile properties. Surprisingly, prior research does not comprehensively explore FSW results to determine safe bending strength and bending toughness for achieving a 900 bend. This paper fills this gap by extensively comparing these properties and investigating welds with varied plate combinations and tool geometries.

The research objective is to enhance the efficiency of the FSW process and to forecast output parameters utilizing input variables, including tool rotations per minute (rpm), tool geometry, and tool pin profile. To achieve this, neural methodologies, specifically the Conventional Feedforward Neural Model (CFNM) and an innovative Flexible Neural Network Model (FNNM), are utilized to model and simulate the FSW process. This research contributes valuable insights into enhancing FSW processes for specific applications, addressing the critical need to understand bending characteristics in aluminum plates for shipbuilding and naval purposes.

2. Method

The experimental study involved various combinations of base materials for Variable Axial Force Friction Stir Welding (VAFSW) joints. The specific combinations included Al 6063 with Al 6063, Al 6063 with Al 5083, Al 5083 with Al 5083, Al 6061 with Al 6061, and Al 6061 with Al 5083. The process was performed at four different tool rpm ranging between 800 rpm to 1400 rpm. Three feed rates, viz 30, 40, and 50 mm/min, were used to produce VAFSW welds. As per the literature review, careful consideration was given to selecting H13 chromium hot-work tool steel with a hardness of 52 HRC for the FSW process using the VAFSW technique. This choice of tool steel aligns with the welding requirements and contributes to the overall success of the experimental investigations. The composition of base metal plates is given in Table 1. The complete practical method is depicted in Fig. 1.

Table 1. Composition of different alloys

Material	Composition								
	Mn	Fe	Mg	Si	Cu	Zn	Ti	Cr	Al
Al6063	0.05	0.6	0.9	0.7	0.3	0.2	0.1	0.25	Rest
Al5083	0.65	0.29	4.55	0.12	0.014	0.006	0.03	0.088	Rest
Al6061	0.15	0.50	0.8	0.4	0.2	0.3	0.15	0.04	Rest

The specimens are prepared with a standard size of 65 mm wide and 6 mm thick, respectively. The design of the portable fixture prioritizes user convenience by incorporating features that simplify the clamping process. Specifically, the fixture is engineered to be effortlessly secured in a vice,

eliminating the necessity for supplementary clamping on the milling machine bed. This strategic design not only streamlines the setup process but also enhances the overall efficiency of operations. The user can easily remove and re-attach the fixture as required, providing high flexibility and adaptability in various machining tasks. This design choice optimizes workflow by minimizing time spent on clamping procedures, making the entire machining process more efficient and user-friendly.

Specific tool parameters are carefully selected in the Friction Stir Welding (FSW) process to ensure optimal performance. The tool configuration includes a shoulder diameter (D) of 16 mm and a pin diameter (d) of 5 mm, maintaining a ratio of $D/d=3:1$ (approximately). The tool pin length is also set at 4.8 mm, representing about 75% of the specimen's thickness. Three distinct tool shapes are employed in FSW, each contributing to different welding characteristics. These shapes are identified as follows: 1. Straight threaded pin (STH), 2. Square pin (SQA), and 3. Pedal pin (PEP). The diverse tool shapes cater to varying welding requirements and are crucial factors in determining the quality and efficiency of the friction stir welding process, as illustrated in Fig. 1. Then, Fig. 2 shows the FSW machine and fixture setup for securing the plate during the process.



Fig. 1. Tools employed for VAFSW process

Specimens were prepared as per ASTM-E8 standard, and the dimensions of the specimen are shown in Fig. 3. Process flow diagram is shown in Fig. 4 where the sequential steps of the research can be viewed. Once the specimens are tested their results are examined and compared. Table 4 shows the results for the Al6063- Al6063 combination. The tool profile change, tool rpm, and tool feed rate variation in tensile strength, bending strength, and bending toughness are obtained. Conventional CFNM and a new FNNM techniques were used to draw comparison and analyzing the best combination of inputs to get desired output.

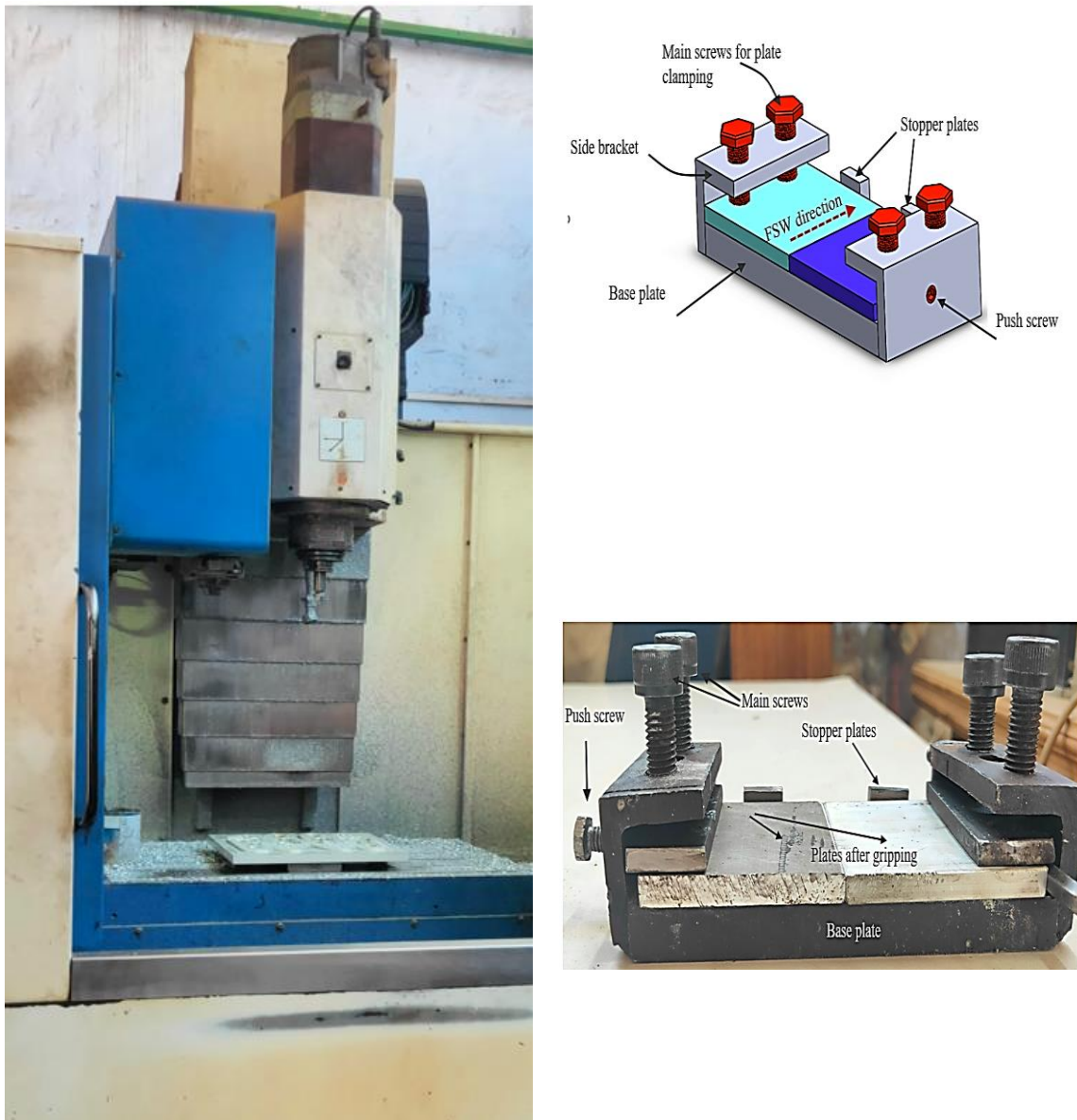


Fig. 2. VAFSW machine and fixture setup

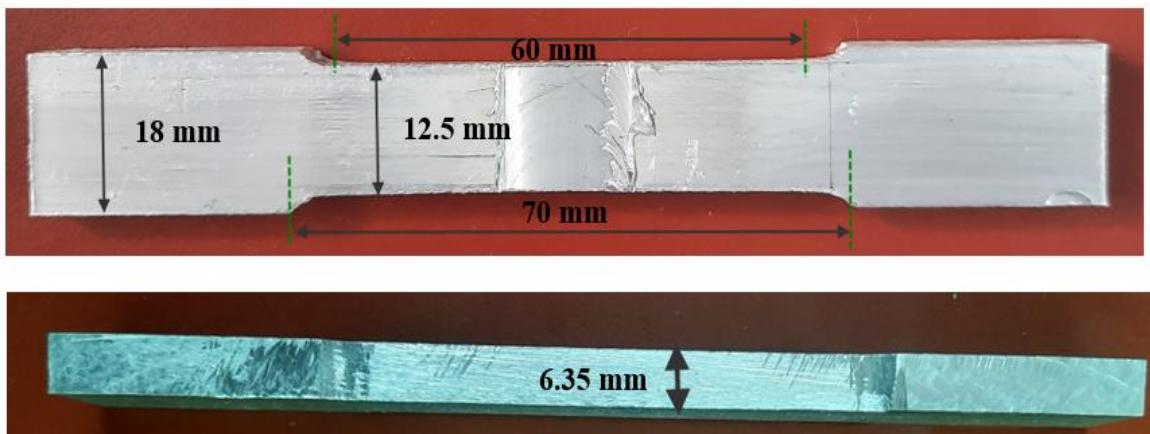


Fig. 3. Different dimensions of specimen used in VAFSW

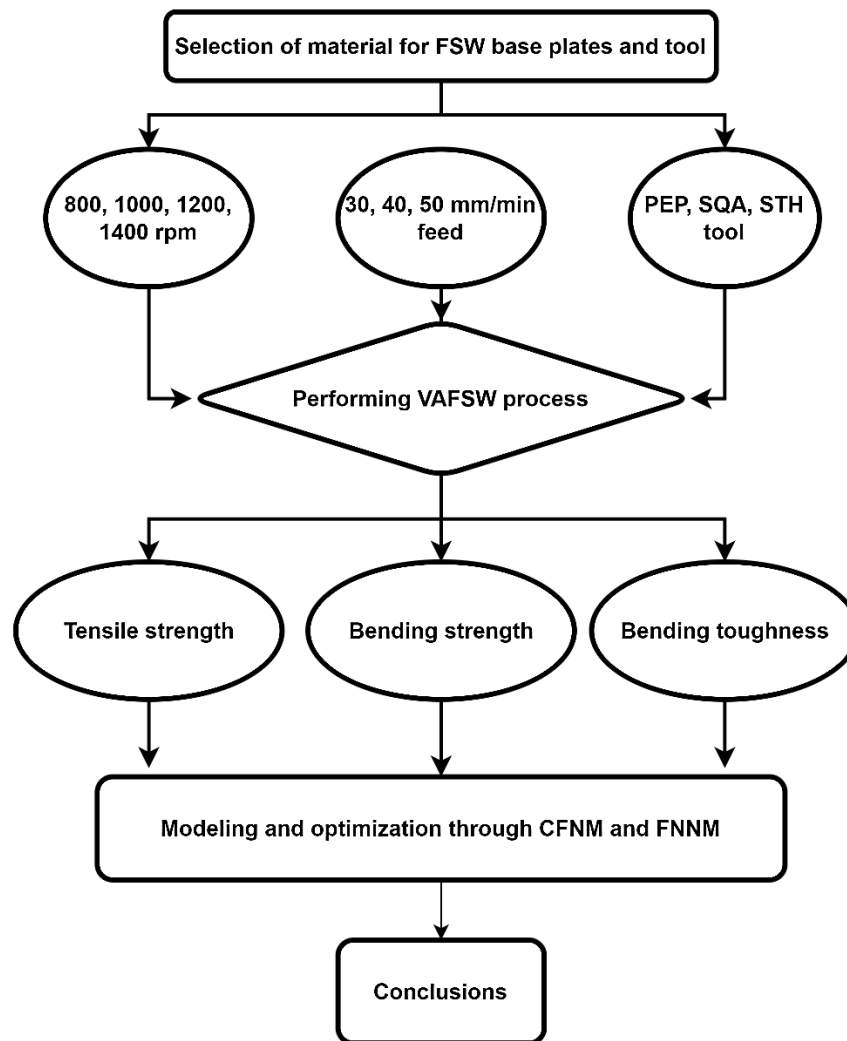


Fig. 4. Process flow diagram

Table 2 shows the results of tensile and bending tests performed on specimen prepared during FSW for 6063-6063 combination and Table 3 shows the results for dissimilar 6063-5083 combination.

Table 2. Results of Al6063-Al6063 FSW using PEP tool

Tool speed (rpm)	Feed (mm/min)	Tensile test results (MPa)	Notch bar test results	
			Bending stress σ_b (MPa)	Toughness (N-m) in 90° bend
800	30	161	210	221
800	40	155	195.4	240
800	50	149	147.6	226
1000	30	146	218.9	280
1000	40	130	214	300
1000	50	126	203	221
1200	30	128	227	298
1200	40	120	233.3	252
1200	50	122	263	344
1400	30	120	251.2	330

Table 3. Results obtained for the dissimilar FSW of Al6063-Al5083

Tool speed	Tool type	Feed	Tensile test results	Notch bar test results	
rpm	(STH, SQA, PEP)	(mm/min)	UTS (MPa)	Bending stress σ_b (MPa)	Toughness (N-m) in 90° bend
800	PEP	30	168	214.3	238
800	PEP	40	155	196.4	210
800	PEP	50	142	177.4	198
1000	PEP	30	153	219.5	280
1000	PEP	40	144	238.2	312
1000	PEP	50	139	381	300
1200	PEP	30	141	252.3	290
1200	PEP	40	134	202.4	290
1200	PEP	50	128	350.4	436
1400	PEP	30	130	172.8	200
1400	PEP	40	133	198.5	196
1400	PEP	50	121	186.8	288
800	SQA	30	138	192.8	208
800	SQA	40	129	200	190
800	SQA	50	127	181	156
1000	SQA	30	122	190.5	202
1000	SQA	40	121	220.2	264
1000	SQA	50	117	214.3	290
1200	SQA	30	137	242.9	310
1200	SQA	40	141	273.8	333
1200	SQA	50	120	255.95	330
1400	SQA	30	118	226.19	266
1400	SQA	40	135	242.85	282
1400	SQA	50	124	280.95	356
800	STH	30	159	217.9	248
800	STH	40	143	193.3	202
800	STH	50	138	184.5	135
1000	STH	30	132	219	274
1000	STH	40	127	232.1	288
1000	STH	50	121	235.2	304
1200	STH	30	136	180.9	212
1200	STH	40	129	195.7	280
1200	STH	50	123	232.1	308
1400	STH	30	120	174.5	188
1400	STH	40	124	187.6	214
1400	STH	50	119	200	294

2.1. Modeling and Simulation of FSW Processes

Similar and dissimilar metals are used in FSW processes for welding, and then the joint strength is tested for tensility and bending. These results are used for model development using a neural approach. The data is arranged in the following format:

- Input data: Tensile strength, Bending strength, and Toughness
- Output data: RPM, Shape of tool, and Feed rate

The total data is divided into three parts, namely

- Training data (70%),
- Validation data (15%), and
- Testing data (15%)

2.1.1 Conventional Feedforward Neural Model (CFNM)

It consists of an input layer and an output layer. In between these layers, some hidden layer(s) is (are) there to cope up the non-linear behavior of the problem.

The number of neurons at input layer equals the number of inputs and the neurons at output layer equals the number of outputs. But, unfortunately, neither number of hidden layers known to the modeler beforehand nor the number of neurons in hidden layer(s) [28,29].

The CFNM neuron, as shown in Fig. 5, has summation as aggregation function, which adds all the inputs after multiplying with their corresponding weights. This aggregated output of the first portion of the neuron is passed through the threshold function to get the final output of the neuron. Threshold functions are sigmoid and linear at hidden and output layers.

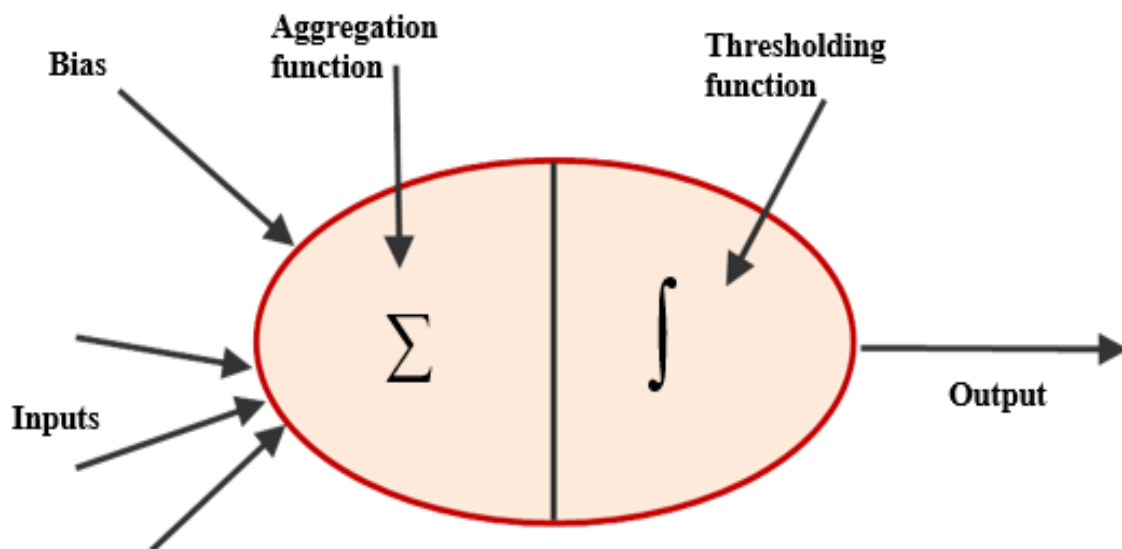


Fig. 5 Conventional neuron used in CFNM

2.1.2 Flexible Neural Network Model (FNNM)

The FNNM has flexibility at both stages in neurons. The aggregation function is not a single function, unlike the CFNM neuron but during training it picks up one or more than one aggregation function(s) from the basket of aggregation functions depending on the complexity of the problem. The aggregation function basket consists of summation, product, arithmetic mean, geometric mean, minimum or maximum of inputs, etc. Similarly, at the next stage of threshold function, it selects one or more than one threshold function(s) from the threshold functions basket to cope up the non-linear

behavior of the problem. The threshold function basket consists of linear, triangular, sigmoid, and Gaussian. Due to this flexibility, FNNM requires only one neuron and one layer as shown in Fig. 6.

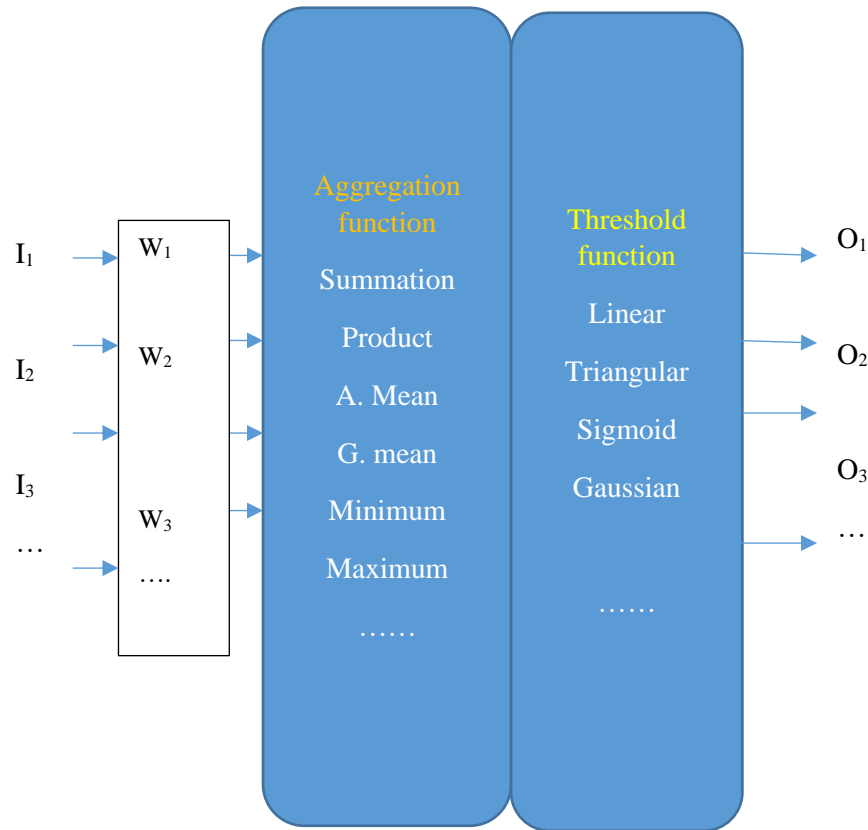


Fig. 6. FNNM neuron

2.1.3 Advantages of FNNM

FNNM requires fewer weights to be adjusted during training compared to CFNNM. By reducing the number of weights, training time, memory requirement, and the training data required decreased.

Calculations of output in FNNM

Step 1) The output of FNNM is calculated as

$$O_j = O_s * W_s + O_{PI} * W_{PI} + O_{AM} * W_{AM} + O_{GM} * W_{GM} + O_{min} * W_{min} + O_{max} * W_{max} \quad (1)$$

Where j=1 to m (number of outputs)

Weight matrix = [W_s W_{PI} W_{AM} W_{GM} W_{min} W_{max}]

Step 2) The output of the summation part of the FNNM is

$$O_s = f(\lambda s * s_{net}) \quad (2)$$

Where $s_{net} = \sum W_{si} X_i + X_{os}$

X_i – inputs i=1 to n (number of inputs)

Step 3) The output of the product part of the FNNM is

$$O_{PI} = f(\lambda_{PI} * pi_net) \tag{3}$$

where $pi_net = \prod W_{PI} X_i * X_{oPI}$

Step 4) The output of the arithmetic mean part of the FNNM is

$$O_{AM} = f(\lambda_{AM} * AM_net) \tag{4}$$

where $AM_net = \frac{1}{(n+1)} \sum_{i=1}^n W_{AMi} X_i * X_{oAM}$

Step 5) The output of the Geometric mean part of the FNNM is

$$O_{GM} = f(\lambda_{GM} * GM_net) \tag{5}$$

where $GM_net = \frac{1}{n+1} \prod_{i=1}^n W_{GMi} X_i * X_{oGM}$

Step 6) The output of the Min part of the FNNM is

$$O_{Min} = f(Min(W_{Min} * Xi)) \tag{6}$$

Step 7) The output of the Max part of the FNNM is

$$O_{Max} = f(Max(W_{Max} * Xi)) \tag{7}$$

Step 8) The error calculation is

$$Ei = (Yi - Oi) \tag{8}$$

Consequently, the total squared error for pattern convergence is:

$$Ep = 0.5 \sum Ei^2 \tag{5}$$

a multiplication factor of 0.5 has been used to simplify the calculations.

Step 9) Reverse pass to modify the connection strength.

(a) Weight associated with the Threshold function outputs of the Generalized Neuron is:

$$W_s(k) = W_s(k-1) + \Delta W_s \tag{6}$$

where $\Delta W_s = \eta \delta_k O_s + \alpha W_s(k-1)$ and $\delta_k = \sum (Yi - Oi)$

Similarly, other weights like W_{PI} W_{AM} W_{GM} W_{min} W_{max} can also be calculated.

(b) Weights associated with the inputs of the summation aggregation function part of the Generalized Neuron are:

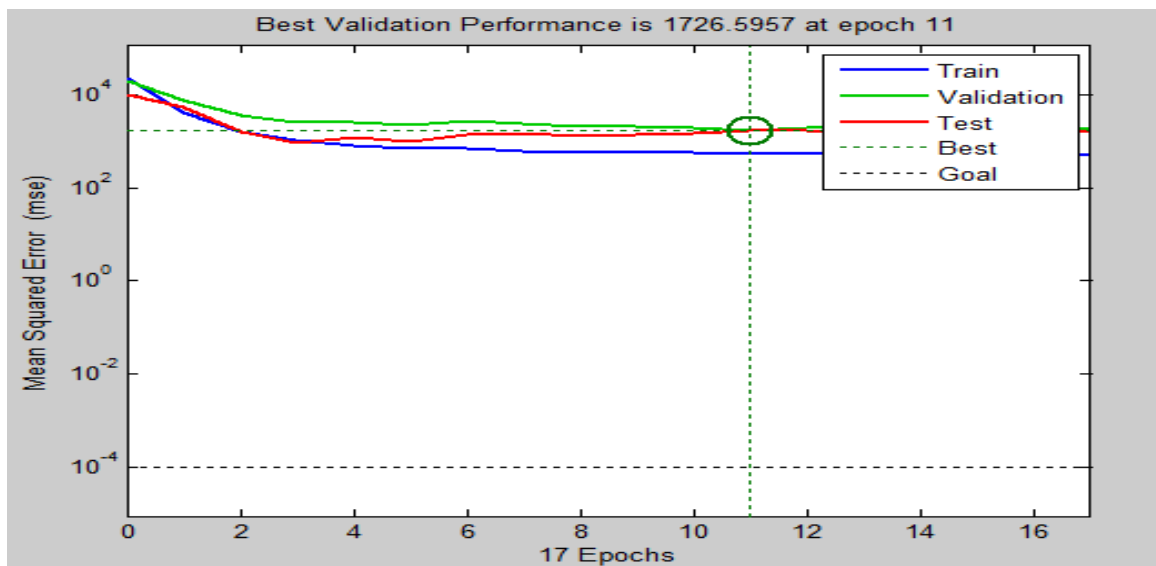
$$W_{\Sigma i}(k) = W_{\Sigma i}(k-1) + \Delta W_{\Sigma i} \tag{7}$$

where $\Delta W_{\Sigma i} = \eta \delta_{\Sigma j} Xi + \alpha W_{\Sigma i}(k-1)$ and $\delta_{\Sigma j} = \sum \delta_k W(1 - O_{\Sigma}) * O_{\Sigma}$

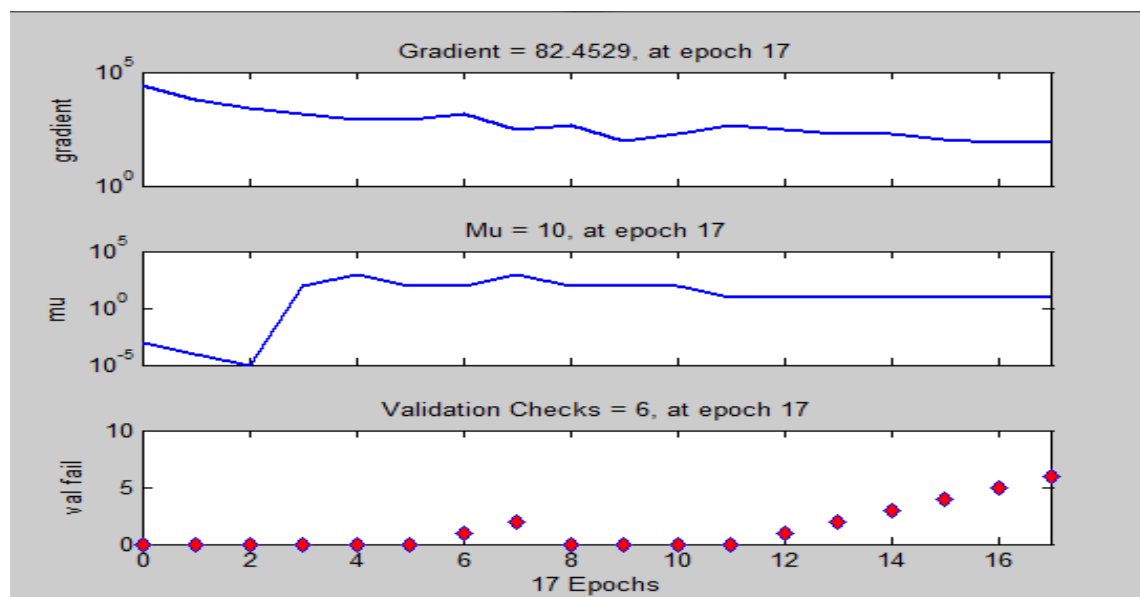
Similarly, other weights related to aggregate functions such as product, arithmetic mean, geometric mean, min, max can also be calculated. Where η is the learning rate and α is the momentum component for improved convergence. Experience determines the range of these parameters, which range from 0 to 1. Both the above-mentioned neural approaches are trained, validated, and tested for the data generated in the FSW processes.

3. Results and Discussion

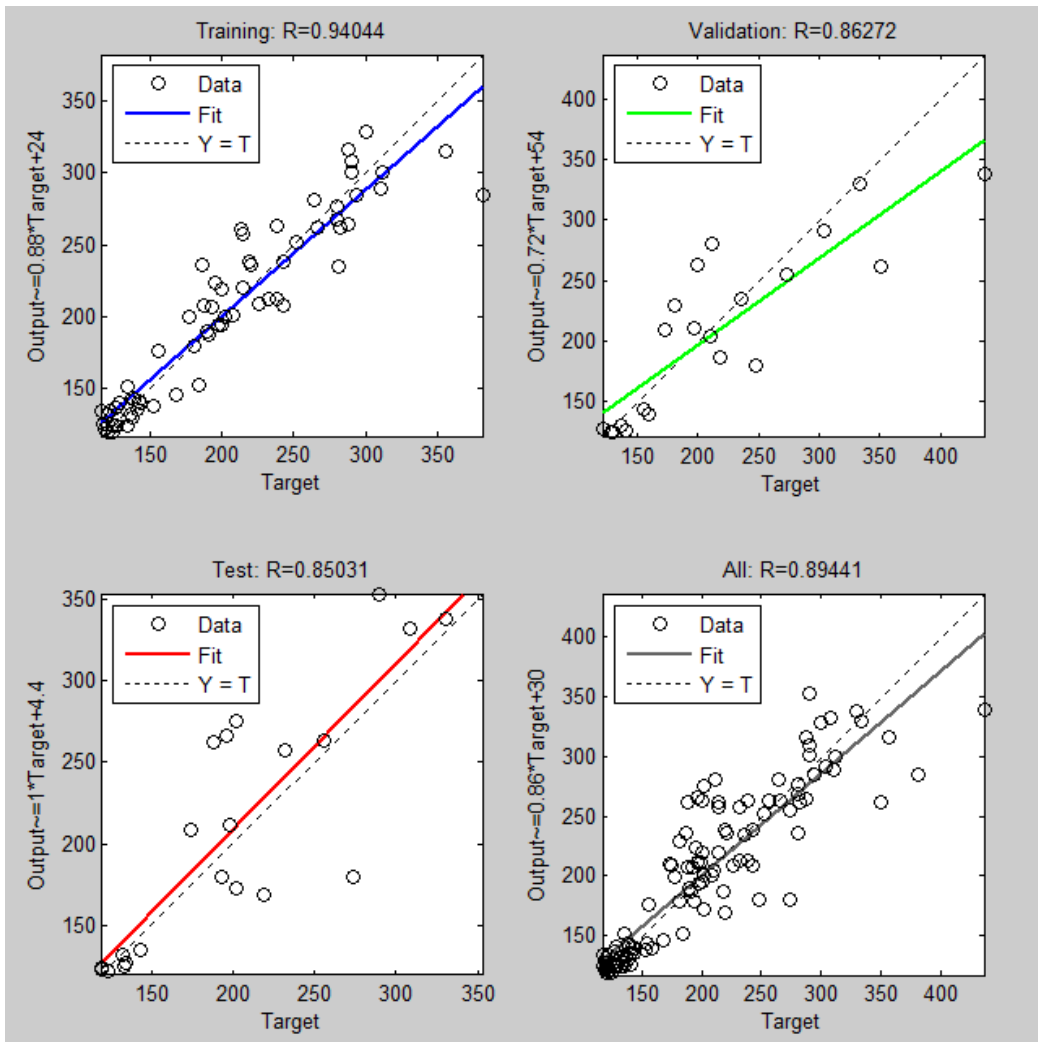
CFNM's training and testing results are shown in Fig. 7. Also, FNNM is trained and tested with the same data. The results of CFNM and FNNM are compared with actual results for dissimilar Al5083-Al6063 welds and shown in Fig. 8 for predicting bending strength, Bending toughness, and UTS. Similarly, Fig. 9-11 gives the comparison of CFNM, FNNM and Actual results for similar alloys/metal welds Al5083-Al5083, Al6063-Al6063, and Al6061-Al6061.



(a) Graph for the best validation performance and the minimum mean squared error (MSE)

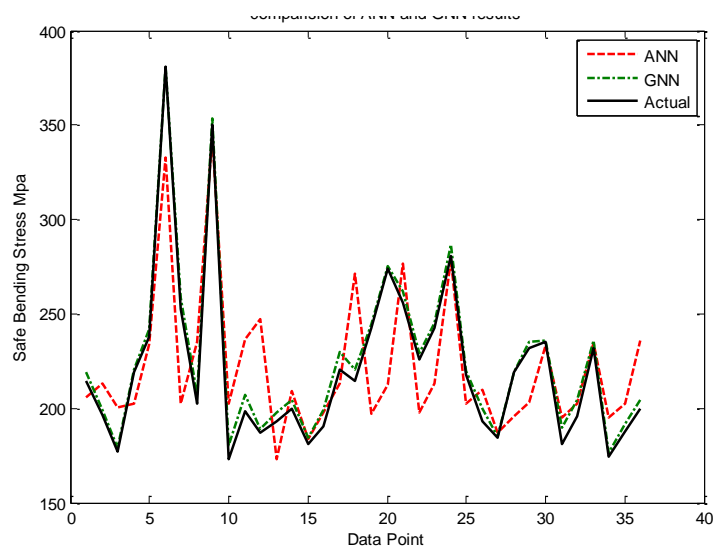


(b) Gradient, momentum, and validation checks (screenshot)

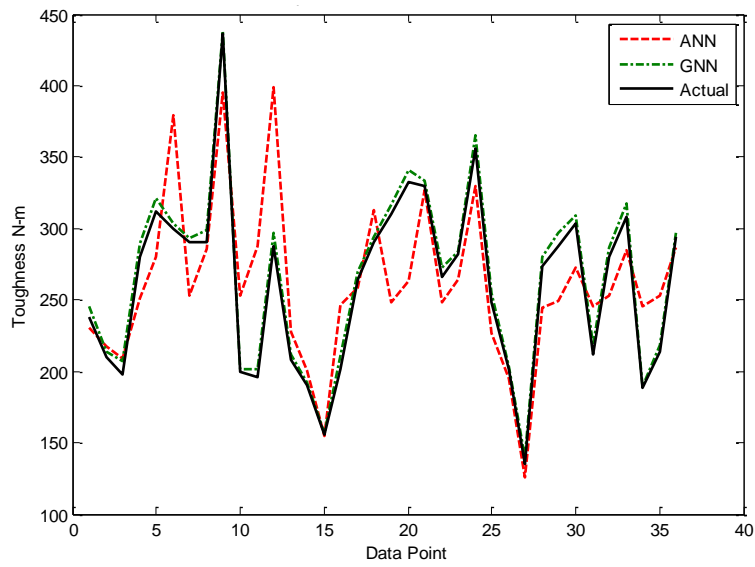


(c) Training performance of ANN model for Al6063-Al5083 VAFSW process (screenshot)

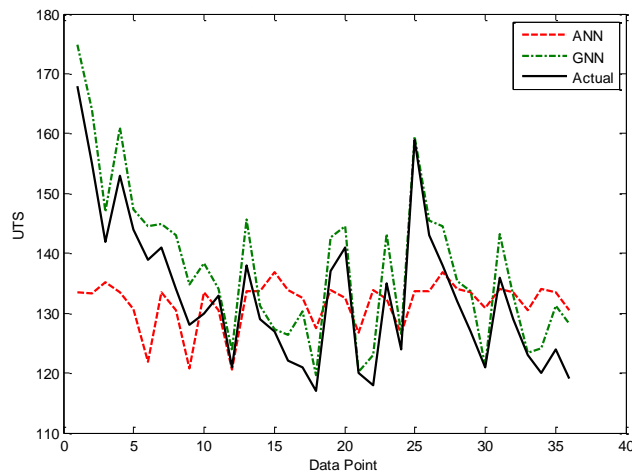
Fig. 7. Training and testing results of CFNM



(a) Comparison of ANN, GNN, and Actual data of bending stress for Al5083-Al6063

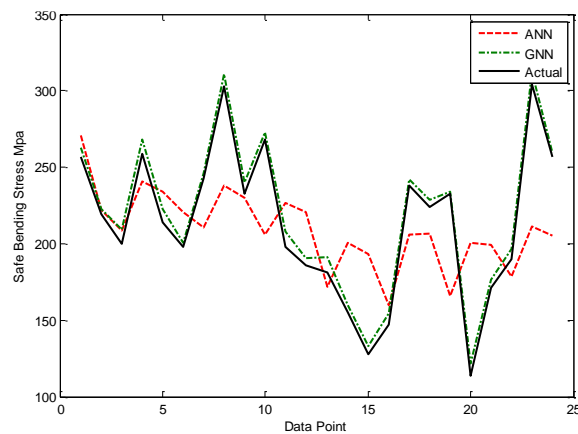


(b) Comparison of ANN, GNN, and actual data of toughness for A15083-A16063

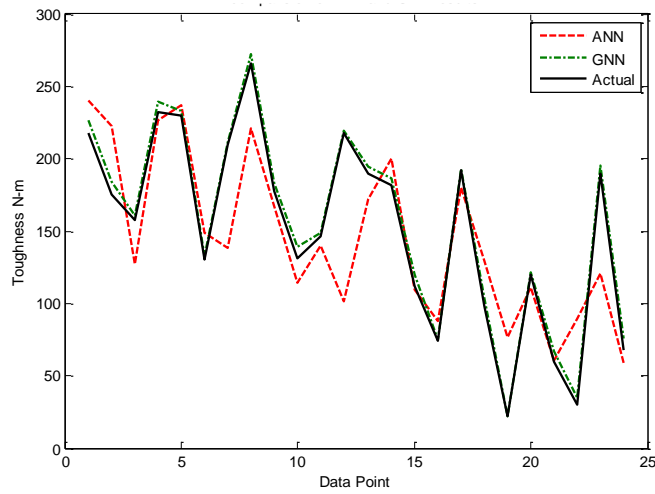


(c) Comparison of ANN, GNN, and actual data of UTS for A15083-A16063

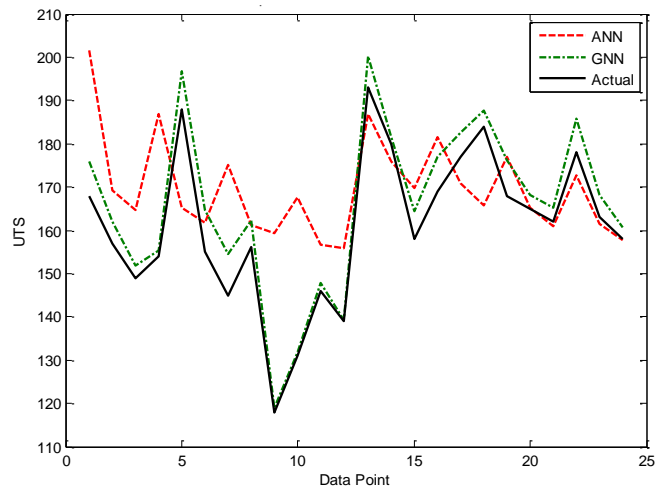
Fig.8. Comparison of ANN, GNN, and actual results for A15083-A16063



(a) Comparison of ANN, GNN, and actual data of bending stress for A15083-A15083

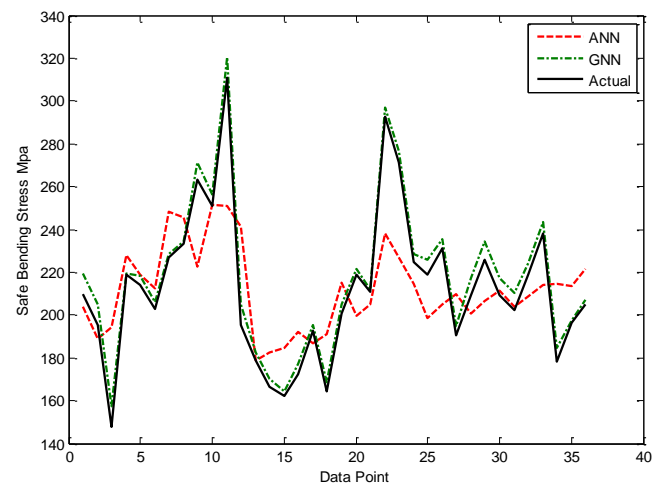


(b) Comparison of ANN, GNN, and actual data of toughness for A15083-A15083

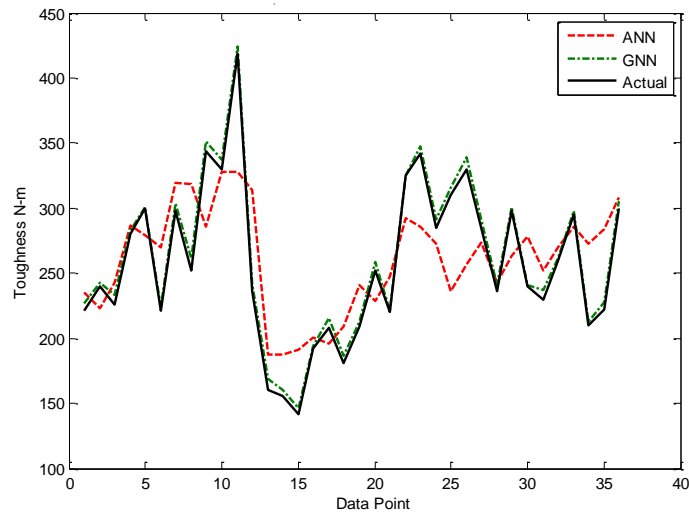


(c) Comparison of ANN, GNN and Actual data of toughness for A15083-A15083

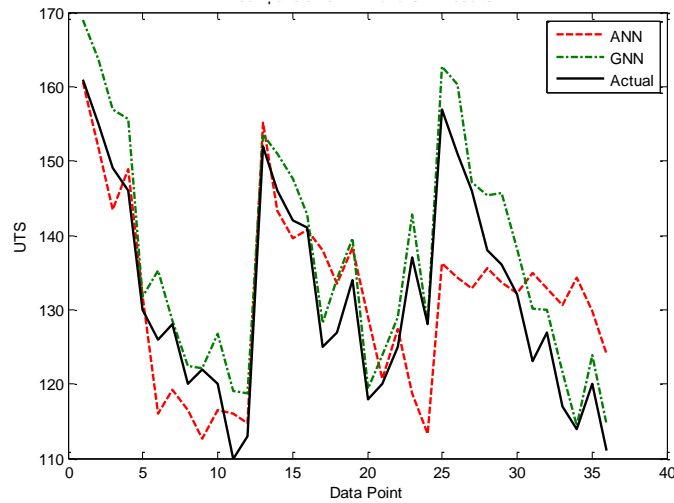
Fig. 9. Comparison of ANN, GNN and actual results for A15083-A15083



(a) Comparison of ANN, GNN and Actual data of bending stress for A16063-A16063

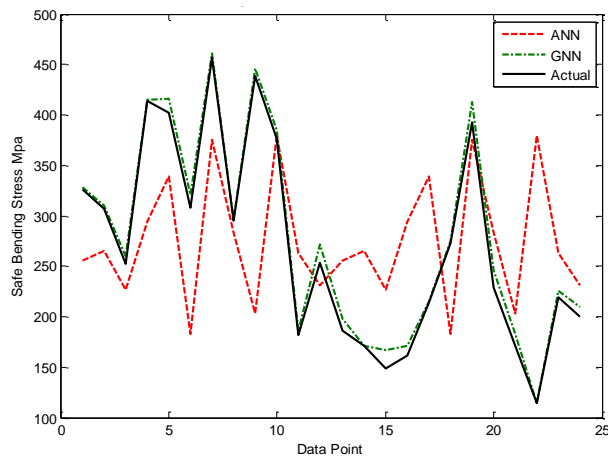


(b) Comparison of ANN, GNN and Actual data of toughness for Al6063-Al6063

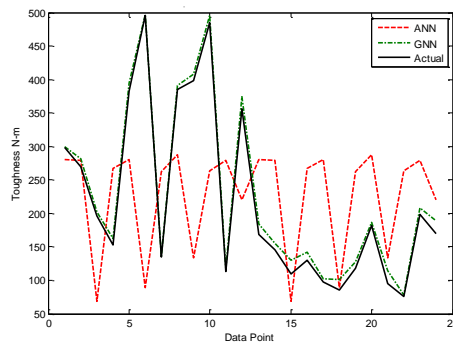


(c) Comparison of ANN, GNN and Actual data of UTS for Al6063-Al6063

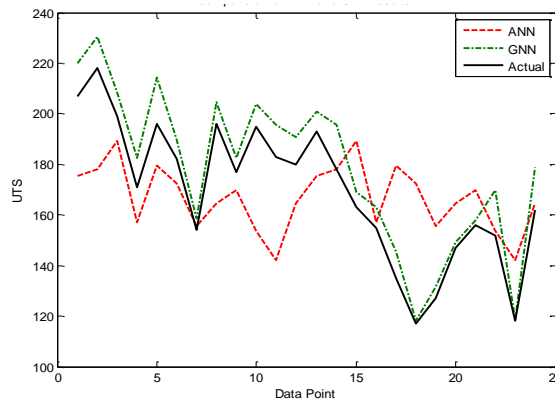
Fig. 10. Comparison of ANN, GNN and actual results for Al6063-Al6063



(a) Comparison of ANN, GNN and Actual data of bending stress for Al6061-Al6061



(b) Comparison of ANN, GNN and Actual data of toughness for Al6061-Al6061



(c) Comparison of ANN, GNN and Actual data of UTS for Al6061-Al6061

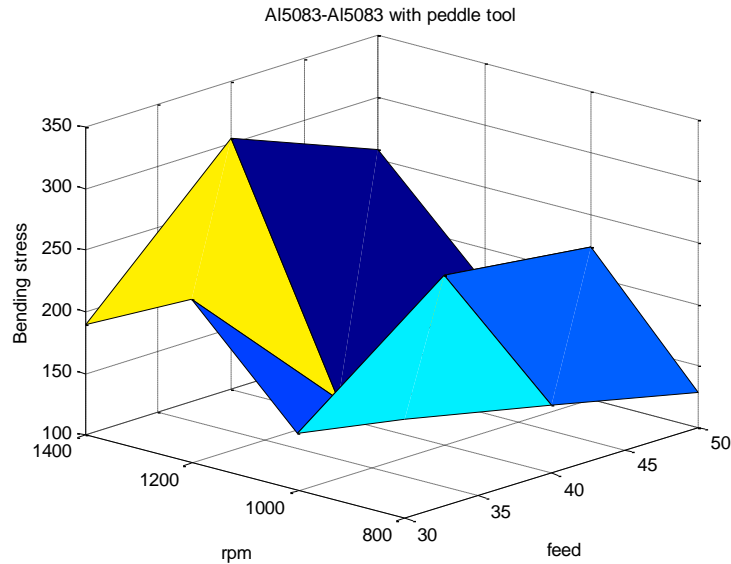
Fig. 11. Comparison of ANN, GNN and actual results for Al6061-Al6061

Table 4 compares the performance of CFNM and FNNM results during test. It shows that RMS error or FNNM is very low in comparison to CFNM. In case of FNNM the results are more than 97% accurate.

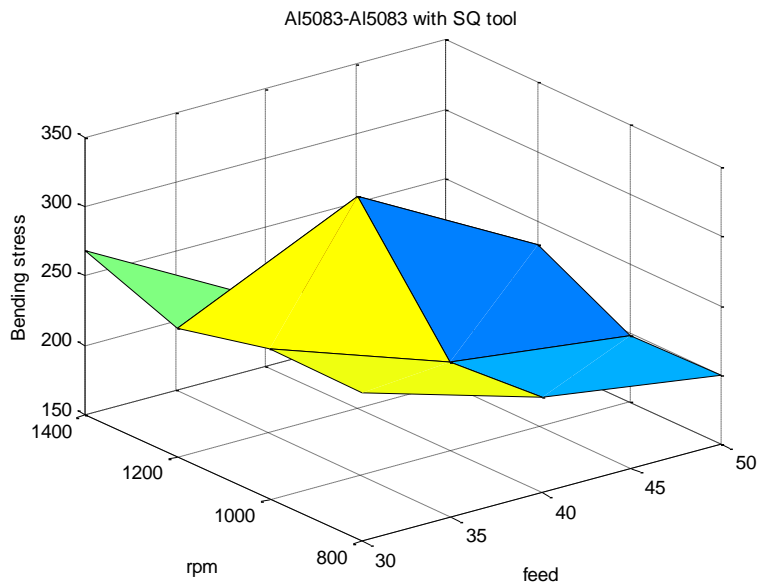
Table 4. Comparison of results of ANN/GNN model

S.No.	Alloy	Techniques	Safe Bending Stress RMSE%	Toughness RMSE %	UTS RMSE %
1	Al5083-Al5083	ANN	14.1980	15.0955	9.6795
		GNN	2.1208	2.0392	2.9707
2	Al5083-Al6063	ANN	7.4440	9.3069	7.0016
		GNN	1.2896	1.4285	3.3249
3	Al6063-Al6063	ANN	8.0531	9.7713	5.9022
		GNN	1.8473	1.3037	3.5667
4	Al6061-Al6061	ANN	7.0855	17.0099	9.0103
		GNN	1.3233	1.1553	1.9173
5	5083-6061	ANN	12.1740	9.9825	23.4053
		GNN	1.5763	3.1440	2.5748

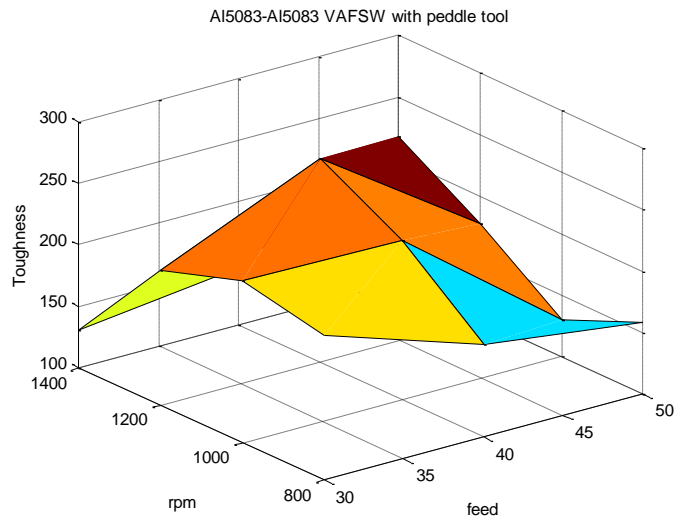
The 3-D meshes are presented in Fig.12 (a-f) below that can represent safe bending stress, toughness and UTS with different tools for 5083-5083 combination of FSW joints. This study introduced a novel Flexible Neural Network Model (FNNM) for the FSW process, achieving significantly higher prediction accuracy for welding outcomes compared to the Conventional Feedforward Neural Model (CFNM). The FNNM demonstrated an RMSE improvement, showcasing its superior capability in handling the complexities of FSW parameter optimization.



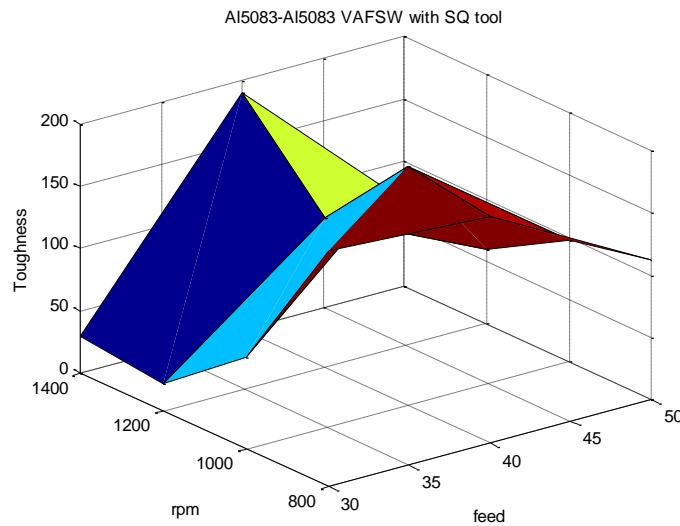
(a) 3-D mesh for Safe Bending stress of VAFSW for PEP tool A15083-A15083



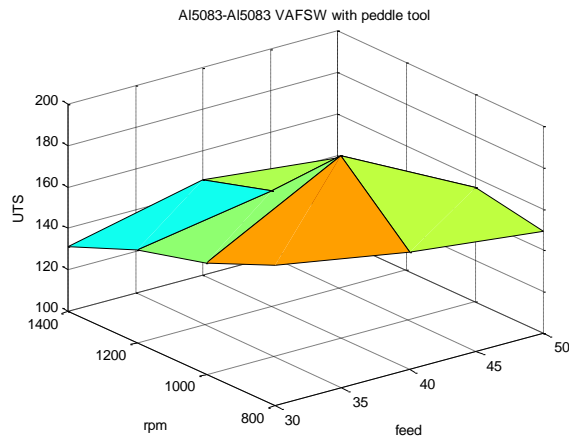
(b) 3-D mesh for Safe Bending stress of VAFSW for SQ tool for A15083-A15083



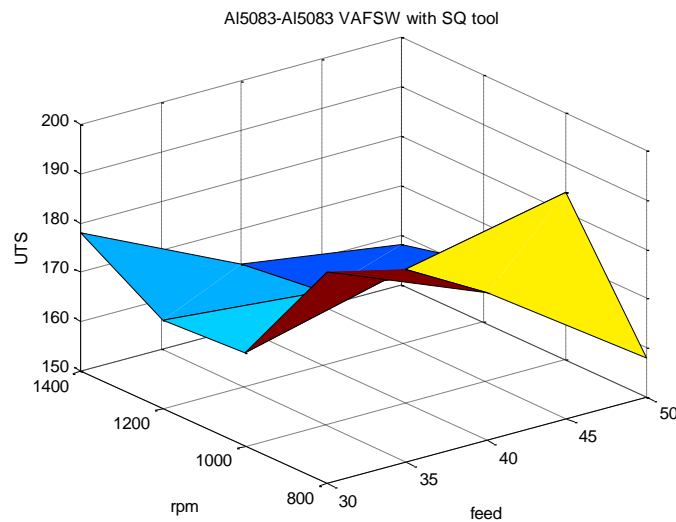
(c) 3-D mesh for Toughness of VAFSW for PEPdle tool for Al5083-Al5083



(d) 3-D mesh for Toughness of VAFSW for SQ tool for Al5083-Al5083



(e) 3-D mesh for UTS of VAFSW for PEPdle tool for Al5083-Al5083



(f) 3-D mesh for UTS of VAFSW for SQ tool for Al5083-Al5083

Fig.12. 3-D meshes for different combinations of Al5083 – Al5083 for predicting mechanical properties of joint.

Unlike previous approaches that largely focused on traditional analytical or less flexible neural network models [31, 33], this study's FNNM offers a novel contribution by dynamically selecting aggregation and threshold functions, which is a significant departure from the rigid structure of CFNM. This flexibility has shown to enhance model performance significantly. The findings suggest that the FNNM's adaptive capabilities could revolutionize the optimization of FSW processes, making it possible to achieve desired welding outcomes with greater efficiency and accuracy. This has broad implications for improving joint quality in critical applications, such as shipbuilding and aerospace, where the precision of welding parameters is paramount.

4. Conclusion

Aluminum plates play a pivotal role in shipbuilding and naval applications, prioritizing bending loads over tensile properties. Remarkably, previous research lacks a thorough investigation into Friction Stir Welding (FSW) results, particularly regarding safe bending strength and bending toughness for achieving a 900 bend. This study addresses this gap by extensively comparing these properties, examining welds with diverse plate combinations and tool geometries.

The research involves similar and dissimilar FSW using different aluminum alloys, namely Al6063, Al6061, and Al5083. Samples, prepared per the ASTM-E8 standard, undergo testing to assess ultimate tensile strength (UTS), safe bending strength, and bending toughness for a 900 bend along the weld line. Given the greater significance of bending strength and toughness over tensile properties, the study seeks optimal input parameters for superior bending and toughness, even at a slight compromise in tensile strength.

In joining Al6063 with Al5083 plates, the best results are achieved using a paddle pin tool (PEP) at 100rpm and a 40mm/min feed rate. This combination yields 144MPa of tensile strength, 238.2 MPa of bending strength, and 312 N-m of toughness for bending the specimen at 90 degrees. The obtained test results are utilized for model development using both Conventional Feedforward Neural Model (CFNM) and a new Flexible Neural Network Model (FNNM) for similar and dissimilar metal joints. FNNM, a novel approach in FSW optimization, demonstrates superior accuracy during training, validation, and testing. 3-D mesh plots are generated to identify required inputs, such as tool

shape, rpm, and feed rate, for obtaining desired outputs, including tensile strength, bending strength, and toughness.

Significant disparities in accuracy between the two models are observed, with a maximum Root Mean Squared Error (RMSE) of 3.5% for FNNM compared to 17% for CFNM. This conclusively highlights the efficacy of FNNM in optimizing the FSW process, predicting results with exceptional accuracy, and determining necessary inputs for desired outputs.

Acknowledgment: The authors would like to express his gratitude towards Prof. P.S. Satsangi, Chairman Advisory committee on Education, Dayalbagh Educational Institutes, Dayalbagh, Agra, U.P. 282005, who is the guiding light for all their research.

References

- [1] M. Sindhuja, S. Neelakrishnan, and B. S. Davidson, "Effect of Welding Parameters on Mechanical Properties of Friction Stir Welding of Dissimilar Metals - A Review," In *IOP conference series: materials science and engineering*, vol. 1185, no. 1, 2021, doi: [10.1088/1757-899X/1185/1/012019](https://doi.org/10.1088/1757-899X/1185/1/012019)
- [2] H.K. Sharma, K. Bhatt, K. Shah, U. Joshi, "Experimental Analysis of Friction Stir Welding of Dissimilar Alloys AA6061 and Mg AZ31 Using Circular Butt Joint Geometry," *Procedia Technology*, vol. 23, pp. 566–572, 2016, doi: [10.1016/j.protcy.2016.03.064](https://doi.org/10.1016/j.protcy.2016.03.064)
- [3] N. R. J. Hyness, M. V. Prabhu, P. S. Velu, R. Kumar, R. Tharmaraj, M. U. Farooq, C. I. Pruncu, "An experimental insight of friction stir welding of dissimilar AA 6061/Mg AZ 31 B joints," *Proceedings of the Institution of Mechanical Engineers, Part B: Journal of Engineering Manufacture*, vol. 236, no. 6–7, pp. 787–797, 2022, doi: [10.1177/09544054211043474](https://doi.org/10.1177/09544054211043474)
- [4] B. Meyghani and C. Wu, "Progress in Thermomechanical Analysis of Friction Stir Welding," *Chinese Journal of Mechanical Engineering*, Springer, vol. 33, 2020, doi: [10.1186/s10033-020-0434-7](https://doi.org/10.1186/s10033-020-0434-7)
- [5] M. Garware, G.T. Kridli, and P.K. Mallick, "Tensile and Fatigue Behavior of Friction-Stir Welded Tailor-Welded Blank of Aluminum Alloy 5754," *Journal of Materials Engineering and Performance*, vol. 19, no. 8, pp. 1161-1171, 2010, doi: [10.1007/s11665-009-9589-1](https://doi.org/10.1007/s11665-009-9589-1)
- [6] M. Sahin, "Joining of Aluminium and Copper materials with Friction," *The International Journal of Advanced Manufacturing Technology*, vol. 49, pp. 527-534, 2010, doi: [10.1007/s00170-009-2443-7](https://doi.org/10.1007/s00170-009-2443-7)
- [7] J. Adamowski and M. Szkodo, "Friction Stir Welds (FSW) of aluminium alloy AW6082-T6," *Journal of Achievements in Materials and Manufacturing Engineering*, vol. 20, pp. 403-406, 2007, Available: www.infona.pl/
- [8] F. Ji, S. Xue, J. Lou, Y. Lou, S. Wang, "Microstructure and Properties of cu/Al Joints Brazed with Zn–Al Filler Metals," *Transactions of Nonferrous Metals Society of China*, vol. 22, no. 2, pp. 281–287, 2012, doi: [10.1016/S1003-6326\(11\)61172-2](https://doi.org/10.1016/S1003-6326(11)61172-2)
- [9] M. Weigl, F. Albert, and M. Schmidt, "Enhancing the Ductility of Laser-Welded Copper-Aluminum Connections by Using Adapted Filler Mater," *Physics Procedia*, vol. 12, pp. 332–338, 2011, doi: [10.1016/j.phpro.2011.03.141](https://doi.org/10.1016/j.phpro.2011.03.141)
- [10] G. Joseph and K. I. C. Kundig, "Copper: Its Trade, Manufacture, Use, and Environmental Status," ASM Int., 1998.
- [11] W. Miller, L. Zhuang, J. Bottema, A. Wittebrood, P. De Smet, A. Haszler, A. J. M. S. Vieregge, "Recent Development in Aluminium Alloys for the Automotive Industry," *Materials Science and Engineering: A*, vol. 280, no. 1, pp. 37–49, 2000, doi: [10.1016/S0921-5093\(99\)00653-X](https://doi.org/10.1016/S0921-5093(99)00653-X)
- [12] G. Joseph and K. I. C. Kundig, "Copper: Its Trade, Manufacture, Use, and Environmental Status," ASM International, 1998, Available: <https://www.osti.gov/>

- [13] S. T. Amancio-Filho, S. Sheikhi, J. F. dos Santos, C. Bolfarini, "Preliminary Study on the Microstructure and Mechanical Properties of Dissimilar Friction Stir Welds in Aircraft Aluminium Alloys 2024-t351 and 6056-t4," *Journal of Materials Processing Technology*, vol. 206, no. 1, pp. 132–142, 2008, doi: [10.1016/j.jmatprotec.2007.12.008](https://doi.org/10.1016/j.jmatprotec.2007.12.008)
- [14] R. Nandan, T. DebRoy, and H. Bhadeshia, "Recent Advances in Friction-Stir Welding – Process, Weldment Structure and Properties," *Prog. Mater. Sci.*, vol. 53, no. 6, pp. 980–1023, 2008, doi: [10.1016/j.pmatsci.2008.05.001](https://doi.org/10.1016/j.pmatsci.2008.05.001)
- [15] M. Ghosh, K. Kumar, S. V. Kailas, and A. K. Ray, "Optimization of Friction Stir Welding Parameters for Dissimilar Aluminum Alloys," *Materials & Design*, vol. 31, no. 6, pp. 3033–3037, 2010, doi: [10.1016/j.matdes.2010.01.028](https://doi.org/10.1016/j.matdes.2010.01.028)
- [16] J. Ouyang and R. Kovacevic, "Material Flow and Microstructure in the Friction Stir Butt Welds of the Same and Dissimilar Aluminum Alloys," *Journal of Materials Engineering and Performance*, vol. 11, no. 1, pp. 51–63, 2002, doi: [10.1007/s11665-002-0008-0](https://doi.org/10.1007/s11665-002-0008-0)
- [17] L. E. Murr, R. D. Flores, J. C. McClure, G. Liu, and D. Brown, "Friction-Stir Welding: Microstructural Characterization," *Material Research Innovations*, vol. 1, no. 4, pp. 211–223, 1998, doi: [10.1007/s100190050043](https://doi.org/10.1007/s100190050043)
- [18] J. H. Cho, D. E. Boyce, and P. R. Dawson, "Modeling Strain Hardening and Texture Evolution in Friction Stir Welding of Stainless Steel," *Materials Science and Engineering: A*, vol. 398, no. 1, pp. 146–163, 2005, doi: [10.1016/j.msea.2005.03.002](https://doi.org/10.1016/j.msea.2005.03.002)
- [19] K. P. Mehta and V. J. Badheka, "Effects of Tilt Angle on the Properties of Dissimilar Friction Stir Welding Copper to Aluminum," *Materials and Manufacturing Processes*, vol. 31, no. 3, pp. 255–263, 2016, doi: [10.1080/10426914.2014.994754](https://doi.org/10.1080/10426914.2014.994754)
- [20] Y. Zhao, S. Lin, and F. Qu, "The Influence of Pin Geometry on Bonding and Mechanical Properties in Friction Stir Weld 2014 Al Alloy," *Materials Letters*, vol. 23, pp. 2948–2952, 2005, doi: [10.1016/j.matlet.2005.04.048](https://doi.org/10.1016/j.matlet.2005.04.048)
- [21] A. Kumar and L. S. Raju, "Influence of Tool Pin Profiles on Friction Stir Welding of Copper," *Materials and Manufacturing Processes*, vol. 27, no. 12, pp. 1414–1418, 2012, doi: [10.1080/10426914.2012.689455](https://doi.org/10.1080/10426914.2012.689455)
- [22] A.P. Reynolds and W. Tang, "Alloy, tool geometry, and process parameter effects on friction stir weld energies and resultant FSW joint properties," in *Friction Stir Welding and Processing*, pp. 15-23, 2001.
- [23] S. Ahmed, R. A. ur Rahman, A. Awan, S. Ahmad, W. Akram, M. Amjad, M. Aamir, and I. Khan, "Optimization of process parameters in friction stir welding of AA5451," 2022, doi: [10.21203/rs.3.rs-1606359/v1](https://doi.org/10.21203/rs.3.rs-1606359/v1)
- [24] M. Aissani, S. Gachi, F. Boubenider, and Y. Benkedda, "Design and Optimization of Friction Stir Welding Tool," *Materials and Manufacturing Processes*, vol. 25, pp. 1199–1205, 2010, doi: [10.1080/10426910903536733](https://doi.org/10.1080/10426910903536733)
- [25] H. Eftekharinia, A. A. Amadeh, A. Khodabandeh, M. Paidar, "Microstructure and wear behavior of AA6061/SiC surface composite fabricated via friction stir processing with different pins and passes," *Rare Metals*, 2016, doi: [10.1007/s12598-016-0691-x](https://doi.org/10.1007/s12598-016-0691-x)
- [26] V. Haribalaji, S. Boopathi, M. Asif, "Optimization of friction stir welding process to join dissimilar AA2014 and AA7075 aluminum alloys," *Materials Today: Proceedings*, 2021, doi: [10.1016/j.matpr.2021.09.499](https://doi.org/10.1016/j.matpr.2021.09.499)
- [27] D. Vijayan and S. V. Rao, "Parametric optimization of friction stir welding process of age hardenable aluminum alloys – ANFIS modeling," *Journal of Central South University*, vol. 23, pp. 1847–1857, 2016, doi: [10.1007/s11771-016-3239-1](https://doi.org/10.1007/s11771-016-3239-1)
- [28] D.K. Chaturvedi, "Modelling and Simulation of Systems using Matlab/Simulink," CRC Press, New York, 2010.
- [29] D.K. Chaturvedi, "Soft Computing Techniques and its Applications in Electrical Engineering," Springer, Berlin, 2008.
- [30] Kasman, "Multi-response optimization using the Taguchi-base d grey relational analysis: a case study for dissimilar friction stir butt welding of AA6082-T6/AA5754-H111," Springer Verlag London, 2013, pp.795–804., doi: [10.1007/s00170-012-4720-0](https://doi.org/10.1007/s00170-012-4720-0)

- [31] M. S. Hasan, M. Akbari, P. Asadi, "Multi-Objective Optimization of Friction Stir Welding Parameters Using FEM and Neural Network," *International Journal of Precision Engineering and Manufacturing*, vol. 15, no. 11, pp. 2351-2356, 2014, doi: [10.1007/s12541-014-0600-x](https://doi.org/10.1007/s12541-014-0600-x)
- [32] F. Badour, N. Merah, A. Shuaib, and A. Bazoune, "Thermo-mechanical finite element model of friction stir welding of dissimilar alloys," Springer-Verlag London, 2014, pp. 607–617, doi: [10.1007/s00170-014-5680-3](https://doi.org/10.1007/s00170-014-5680-3)
- [33] H.D. Naghibi, M. Shakeri, M. Hosseinzadeh, "Neural Network and Genetic Algorithm Based Modeling and Optimization of Tensile Properties in FSW of AA 5052 to AISI 304 Dissimilar Joints," *The Indian Institute of Metals - IIM*, 2015, pp. 891–900, doi: [10.1007/s12666-015-0572-2](https://doi.org/10.1007/s12666-015-0572-2)
- [34] S. K. Gupta, K. N. Pandey, R. Kumar, "Artificial intelligence-based modelling and multi-objective optimization of friction stir welding of dissimilar AA5083-O and AA6063-T6 aluminium alloys," In *Proceedings of the Institution of Mechanical Engineers, Part L: Journal of Materials: Design and Applications*, 2016, pp.1–10, doi: [10.1177/1464420715627293](https://doi.org/10.1177/1464420715627293)
- [35] D. Vijayan and S. V. Rao, "Parametric optimization of friction stir welding process of age hardenable aluminum alloys – ANFIS modeling," *Journal of Central South University*, vol. 23, pp. 1847–1857, 2016, doi: <https://doi.org/10.1007/s11771-016-3239-1>
- [36] M.V.R. Durga Prasad and K.K. Namala, "Process Parameters Optimization in Friction Stir Welding by ANOVA," *Materials Today: Proceedings*, vol. 5, pp. 4824–4831, 2018, doi: [10.1016/j.matpr.2017.12.057](https://doi.org/10.1016/j.matpr.2017.12.057)
- [37] K. N. Wakchaure, A. G. Thakurb, V. Gadakh, and A. Kumar, "Multi-Objective Optimization of Friction Stir Welding of Aluminium Alloy 6082-T6 Using hybrid Taguchi-Grey Relation Analysis- ANN Method," *Materials Today: Proceedings*, vol. 5, pp. 7150–7159, 2018, doi: [10.1016/j.matpr.2017.11.380](https://doi.org/10.1016/j.matpr.2017.11.380)
- [38] T. Srichok, R. Pitakaso, K. Sethanan, W. Sirirak, and P. Kwangmuang, "Combined Response Surface Method and Modified Differential Evolution for Parameter Optimization of Friction Stir Welding," *Processes*, vol. 8, 1080, 2020, doi: [10.3390/pr8091080](https://doi.org/10.3390/pr8091080)
- [39] A. Kubit, T. Trzepieciński, R. Kluz, K. Ochałek, and J. Slota, "Multi-Criteria Optimisation of Friction Stir Welding Parameters for EN AW-2024-T3 Aluminium Alloy Joints," *Materials*, vol. 15, 5428, 2022, doi: [10.3390/ma15155428](https://doi.org/10.3390/ma15155428)
- [40] K. Suganeswaran, P. Muthukumar, R. Sathiskumar, R. Parameshwaran, and N. Nithyavathy "Evaluation of microstructural, tribological and tensile characteristics of AA7075 surface composites fabricated through friction stir process," In *Proceedings of the Institution of Mechanical Engineers, Part E: Journal of Process Mechanical Engineering*, 2023, doi: [10.1177/09544089231170987](https://doi.org/10.1177/09544089231170987)